UC Irvine
UC Irvine Previously Published Works

Title
Alkyne Tags for Multiplexed, Optical Photothermal Infrared Imaging of Cellular Metabolites

Permalink
https://escholarship.org/uc/item/3xr4x3d9

Journal
ACS Chemical Biology, 21(8)

ISSN
1554-8929

Authors
Lin-Jones, HalleyM
Hoang, Tuyet
Li, Yong
et al.

Publication Date
2026-08-21

DOI
10.1021/acschembio.6c00300

Copyright Information
This work is made available under the terms of a Creative Commons Attribution License, available at https://creativecommons.org/licenses/by/4.0/

Peer reviewed

eScholarship.org Powered by the California Digital Library
University of California

pubs.acs.org/acschemicalbiology

Letter

Alkyne Tags for Multiplexed, Optical Photothermal Infrared Imaging of Cellular Metabolites

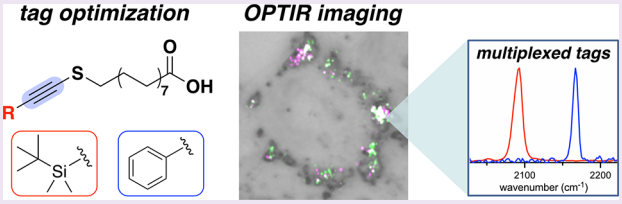
Halley M. Lin-Jones, Tuyet Hoang, Yong Li, Katherine M. Townsend, Shelbee K. Botello, Eric O. Potma,* and Jennifer A. Prescher*

Cite This: *ACS Chem. Biol.* 2026, 21, 1891−1896

Read Online

ACCESS | Metrics & More | Article Recommendations | Supporting Information

ABSTRACT: Optical photothermal infrared (OPTIR) microscopy has emerged as a powerful strategy for vibrational imaging within complex cellular environments. This platform offers subcellular resolution without the diffraction limits of traditional IR. However, the potential for high-level multiplexing has been slowed by a lack of optimized, IR-active bioorthogonal probes. Building on our previous success with sulfur-linked alkyne tags for Raman imaging, we report a panel of compact, sulfur-linked IR-vibrational probes. These motifs feature strategic chemical modifications to maximize n-π^* and d-π interactions, effectively activating the infrared transition dipole of the alkyne moiety. We validated the tools by labeling model lipid targets in cells, demonstrating that the probes exhibit robust, spectrally resolvable signals. This new library of bioorthogonal tags significantly broadens the analytical capabilities of OPTIR, providing a scalable framework for highly multiplexed, high-sensitivity metabolic imaging.



Compact bioorthogonal tags, such as simple alkyne and azide motifs, are versatile tools for monitoring cellular metabolism when affixed to sugars, lipids, and other metabolites.[1] Conventional visualization of the tags exploits covalent chemistries to attach dyes or other optical reporters. These reactions can be chemically challenging, and the resulting probes can further perturb the biomolecules under study. Sterically bulky dyes can alter the diffusive properties of the target molecule and interfere with native cellular processes. Additionally, fluorescent tag delivery via click reactions can require extensive washout steps to remove background signal,[2] impeding real-time tracking of some target biomolecules.

Direct visualization of bioorthogonal tags via their intrinsic vibrational signatures offers a minimally invasive alternative. Because common bioorthogonal motifs exhibit substantial Raman cross sections,[3] they are excellent targets for stimulated Raman scattering (SRS) microscopy.[4−6] SRS combines Raman sensitivity with rapid image acquisition, enabling dynamic tracking of tagged biomolecules in live cells without the need for secondary labeling. The direct visualization approach has already provided important insights into lipid localization, drug distribution, and other key biological processes.[7−9]

A notable advantage of Raman-active probes is their narrow spectral line width compared to the fluorescence emission spectra of organic dyes, rendering them excellent choices for multiplexed imaging. Indeed, structural tuning of alkyne and nitrile probes has provided a broad palette of distinguishable Raman-based tags.[10−13] Recent panels have enabled simultaneous imaging of 14 distinct targets, with extended libraries now reaching up to 24 distinct signals, far surpassing the multiplexing limits of traditional fluorescence microscopy. Despite the growing number of tag motifs for Raman imaging, their utility is limited by the low scattering cross sections inherent to the Raman effect. With molecular detection sensitivities in the millimolar range, Raman microscopy remains unable to detect low-abundance or highly dispersed biomolecules against background contributions. While strategies such as extended alkyne conjugation and nanoparticle encapsulation can amplify these signals,[8,11] they introduce substantial steric bulk that may perturb native biological activity.

Infrared (IR) absorption methods offer a compelling alternative, benefiting from cross sections that are orders of magnitude higher compared to Raman. Although traditional IR imaging was long hindered by poor spatial resolution, optical photothermal infrared (OPTIR) microscopy has overcome the IR diffraction limit, enabling high-sensitivity vibrational imaging with submicron lateral resolution.[14−16] OPTIR has been applied to metabolic studies using compact nitrile and azide tags to track lipid and sugar metabolism in a variety of cell and tissue models.[17−20] Similarly, nitrile-tagged caspase and phosphatase substrates have enabled OPTIR monitoring of enzymatic activity.[21] However, the expansion of the OPTIR toolkit is currently stalled by a lack of IR-specific probes.

Received: March 27, 2026
Revised: July 12, 2026
Accepted: July 14, 2026
Published: July 22, 2026



ACS Publications

© 2026 American Chemical Society

https://doi.org/10.1021/acschembio.6c00300
ACS Chem. Biol. 2026, 21, 1891−1896

Downloaded from pubs.acs.org/acbcct/article-pdf/21/8/1891/6163245/acschembio.6c00300.pdf by UNIV OF CALIFORNIA IRVINE user on 06 November 2026

Because Raman and IR imaging follow different selection rules, Raman-optimized tags, such as polyynes, often perform poorly in IR applications. Although up to three-color OPTIR imaging has been demonstrated,[17] current probes are frequently hindered by signal overlap or insufficient signal intensity. Consequently, there is a need for IR-optimized probes that provide robust, resolvable signals within the cell-silent spectral region to unlock the full potential of high-sensitivity IR-based vibrational imaging.

In this work, we address the shortage of infrared-specific probes by developing a series of versatile motifs characterized by high IR-responsivity, narrow line widths, and precise spectral tunability. Our approach builds on our previous development of sulfur-linked alkynes for Raman imaging.[22] In those studies, we demonstrated that n−π conjugation via a sulfur linker significantly enhances the Raman cross-section of the alkyne mode. The sulfur atom also provides thermal insulation that sharpens the alkyne vibrational line width by reducing intramolecular relaxation. We hypothesized that these same scaffolds could be repurposed and optimized for IR applications. While the alkyne stretch is inherently IR-silent in isolation, we successfully activated the mode by modifying its local chemical environment. By leveraging electron sharing between the lone pairs of sulfur (or selenium) and the empty π*-orbitals of the alkyne, we substantially increased the transition dipole moment. To further amplify and resolve these signals, we engineered a panel of four distinct probes utilizing aryl and silyl substituents alongside heavy-isotope incorporation. We validated these optimized tags by synthesizing palmitic acid conjugates and monitoring their metabolic uptake and storage in cells via OPTIR microscopy. Our results confirm that these sulfur-linked probes provide the robust, resolvable signals necessary for enhanced IR metabolic imaging.

As noted above, our previous work established that sulfur-modified alkyne probes with silyl and phenyl substituents produced spectrally separated Raman signals in the cell-silent region.[22] Additionally, the sulfur-linked phenyl probe (**Ph-Alk-S**) showed a 1.4-fold enhancement in Raman intensity compared to the probe lacking the key sulfur motif (**Ph-Alk**). Based on these promising findings, we first explored whether repurposing sulfur-linked phenyl and silyl probes for OPTIR imaging would yield similarly strong, distinguishable IR signals. We prepared two sulfur-linked alkynyl probes (**Ph-Alk-S** and **TBDMS-Alk-S**) and their sulfur-free analogs (**Ph-Alk** and **TBDMS-Alk**) and compared their OPTIR-derived IR response (Figure 1A).

First, **Ph-Alk** showed no discernible IR response, underscoring that the alkynyl mode retains its highly symmetric character even in the presence of π-conjugation with the substituted phenyl ring. We thus inferred that π-conjugation alone is insufficient to activate the IR response of the alkyne moiety. Second, the introduction of a sulfur linker significantly alters the electron density near the alkyne bond through n-π* bonding with sulfur. This interaction switches on the mode's IR-activity, resulting in a relatively strong IR absorption at 2167 cm^{-1}.

Unlike the **Ph-Alk** tag, the sulfur-free **TBDMS-Alk** exhibits an intrinsic IR response at 2173 cm^{-1}. This suggests that the interaction between the alkyne's π-orbitals and the empty d-orbitals of silicon provides an enhancement mechanism for the alkyne's IR-resonance.[23] The incorporation of an insulating sulfur atom, forming **TBDMS-Alk-S**, enhanced the IR signal

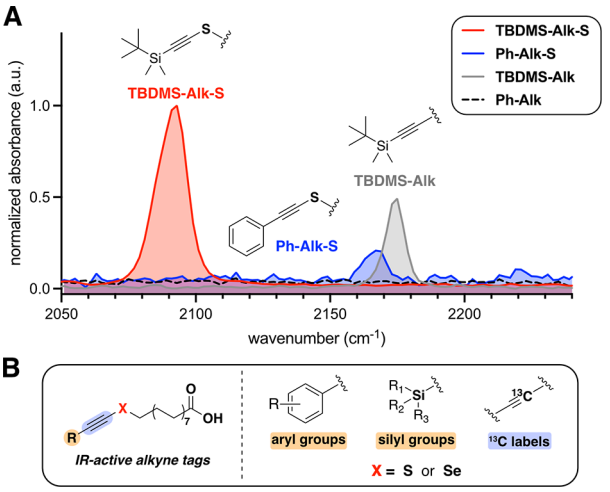


Figure 1. (A) Structures and normalized IR spectra of sulfur-linked alkyne tags (**TBDMS-Alk-S** & **Ph-Alk-S**) and the parent alkyne tags (**TBDMS-Alk** & **Ph-Alk**); (B) Overview of IR-active alkyne tags explored herein, with varied (i) aryl and silyl substituents, (ii) alkyne isotopic labels, and (iii) insulator atoms (S, Se).

intensity by a factor of 2 relative to **TBDMS-Alk** (Figure 1A), while also red-shifting the mode frequency to 2093 cm^{-1}. This red shift is in alignment with our previous Raman measurements, suggesting an overall weakening of the alkyne bond due to increased electron density in its π*-orbitals.

To further expand multiplexing capabilities, we designed a series of alkyne-based tags with structural modifications aimed at shifting IR resonance frequencies. Three strategies were explored to tune the alkyne stretching frequency: (i) substitution at the alkyne terminus, (ii) isotopic labeling, and (iii) modification of the core linker atoms (Figure 1B). The overall goal was to develop 4−5 distinct alkyne tags with a minimal spacing of 20 cm^{-1} between signals for facile multiplexing.

We first designed a series of substituted aryl alkynes to examine the effect of extended π-systems and electron-withdrawing groups on the IR frequency (Figure 2A). The tags were conjugated to palmitic acid using our previously reported two-step synthesis. We hypothesized that the introduction of electron-withdrawing fluorine groups as aryl substituents would red-shift the vibrational signals compared to **Ph-Alk-S**. Additionally, we explored the effect of π-

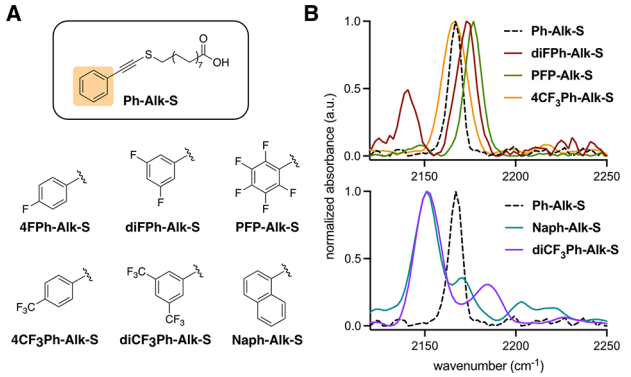


Figure 2. (A) Overview of aryl alkyne tags and (B) measured IR spectra, normalized to the C−H stretch frequency.

Downloaded from pubs.acs.org/acbcct/article-pdf/21/8/1891/6163245/acschembio.6c00300.pdf by UNIV OF CALIFORNIA IRVINE user on 06 November 2026

https://doi.org/10.1021/acschembio.6c00300
ACS Chem. Biol. 2026, 21, 1891−1896

extension of the scaffold through a naphthalene analog, **Naph-Alk-S**.

We next measured the IR frequencies of the individual aryl alkyne tags (Figure 2B). Surprisingly, we observed no detectable IR signal over background in the cell-silent region for the singly fluorinated tag, **4FPh-Alk-S**. Signals were observed with tags comprising additional electron-withdrawing fluorine substituents or a trifluoromethyl unit, but with minimal frequency shifts and substantial overlap with the parent **Ph−Alk−S** band. One exception was with the doubly trifluoromethylated variant (**diCF$_3$Ph-Alk-S**), which displayed a 16 nm red shift in IR spectra from **Ph-Alk-S**. Interestingly, the π-extended probe (**Naph-Alk-S**) generated a similar spectral shift to 2151 cm^{-1}.

Motivated by the intense IR response of the silyl probe, we also prepared tags with varied silyl groups and measured the IR frequencies of the alkynyl stretching mode (Figure 3). The full

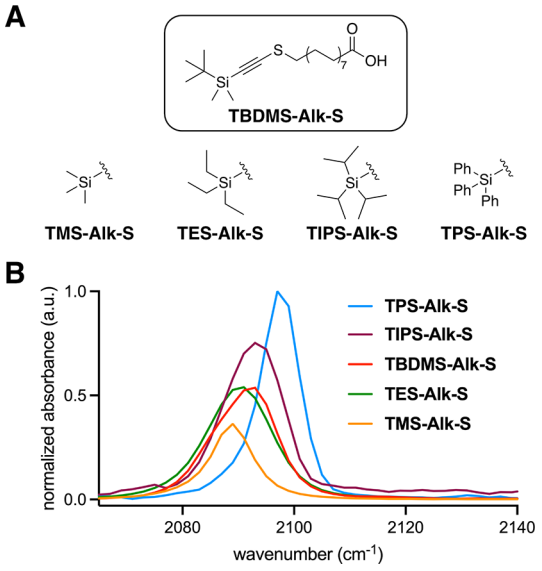


Figure 3. (A) Overview of silyl alkyne tags and (B) measured IR spectra, normalized to the C−H stretch frequency.

panel of silyl-substituted tags produced overlapping IR signals at 2091−2093 cm^{-1}, suggesting that the alkyne stretching vibration in the Si−Alk−S scaffold is relatively insensitive to substitutions at the silicon center. Due to the minimal spectral shift across silyl groups, we moved forward with **TBDMS-Alk-S** for imaging because it is well tolerated by cells (Figure S1). The robustness of the Si-Alk-S mode, while limited in terms of spectral diversity, highlights the stability and reliability of the **TBDMS-Alk-S** tag for vibrational imaging applications. Overall, these silyl tags exhibit the strongest IR signals across the synthesized tag panel (Table S1) and could be broadly useful for sensitive OPTIR imaging.

Given the limited impact of the explored R-groups on alkyne vibrational frequencies, we turned to core modifications at the key alkyne carbons and the insulator atoms. Two tags were prepared with carbon-13 incorporation, a well-established strategy to predictably red-shift the alkyne vibrations. A single carbon-13 incorporation in the phenyl tag (**^{13}CPh-Alk-S**) generated a distinct IR absorption band at 2133 cm^{-1}, while a doubly carbon-13 modified silyl tag (**$^{13}C_2$TMS-Alk-S**) produced a sharp peak at 2008 cm^{-1}. In both cases, the resulting signals were well-resolved and maintained sufficient intensity for OPTIR measurements. Based on DFT calculations, we also envisioned that substitution of the sulfur linker with a selenium atom could provide an additional boost in signal intensity, given the greater electron density (Figure S2). We prepared a compact Se-linked alkyne (**Ph-Alk-Se**) to test this idea. Surprisingly, we only observed a minor 10 nm red shift in the IR signal relative to **Ph-Alk-S**.

From our targeted probe panels, four tags emerged with utility for tandem imaging: **Ph-Alk-S**, **TBDMS-Alk-S**, **^{13}CPh-Alk-S**, and **$^{13}C_2$TMS-Alk-S**. These probes produce spectrally distinct IR signals, each positioned in the cell-silent region (1800−2800 cm^{-1}). As shown in Figure 4A, the absorption peaks are sharp and nonoverlapping and thus well suited for multiplexed detection.

With the alkynyl stretching mode as their core, the IR-tag motifs retain their strong Raman response, allowing a rapid assessment with SRS imaging. To examine cellular uptake of the newly designed tags, the corresponding palmitic acid conjugates were incubated with HeLa cells and imaged using SRS microscopy. All the tested tags, except for **TPS-Alk-S**, were taken up by cells and visible in lipid droplet structures (Figure S3−S4). **TPS-Alk-S** was poorly membrane-permeable and showed a detectable signal only in cells when delivered via liposomal encapsulation (see Methods). With the exception of the TMS-modified probes, the tags were tolerated at doses up to 100 μM (Figure S1), a standard concentration for imaging studies. The trimethylsilyl tags, **TMS-Alk-S** and **$^{13}C_2$TMS-Alk-S**, displayed higher cytotoxicity at lower concentrations. These results suggest that less sterically hindered silyl groups are unstable and are potentially prone to forming toxic adducts in cells. Similar to other studies using vibrational metabolic tags,[17,19,24] we found that extended incubation periods (24−72 h) provided enhanced detection (Figure S5). The tag signal could also be competed with unlabeled palmitic acid (Figure S6), suggesting it has similar activity to the native lipid in cells.

The utility of the spectrally engineered IR probes for OPTIR imaging is illustrated in Figure 4B. Cells were incubated with the palmitic acid probes for 2−4 days and fixed before imaging. Tagged compounds were then visualized with OPTIR by tuning the IR frequency to the alkyne resonance frequency of the respective tag. The bright **TBDMS-Alk-S** tagged probe, visualized at 2093 cm^{-1}, is shown in panel c. The compound was found to accumulate in distinct regions of the cell. The tag signal displayed some overlap with the signal recorded at 2853 cm^{-1} (a generic marker for lipids), suggesting that at least a portion of the palmitic acid probe was metabolized and stored in intracellular lipid droplets. Similar behavior was observed for the **Ph-Alk-S**, **^{13}CPh-Alk-S**, and **$^{13}C_2$TMS-Alk-S** probes, which were mapped at their well-separated vibrational frequencies. Some of the tagged lipids also localized in similar regions of the cell as palmitic acid-d$_{31}$, a well-known vibrational probe known to accumulate in lipid droplets (Figure S7). However, we were unable to retrieve the alkynyl lipids to fully analyze the metabolic end products and potential mechanisms for degradation.

In this work, we systematically examined the IR activity of the alkyne stretching mode by modulating its immediate chemical environment. Our findings reveal several useful design principles for vibrational probe development. First, while π-conjugation with aryl groups profoundly enhances the Raman response, we found its effect on IR activity to be minimal. This observation aligns with the fundamental differences between Raman and IR transitions: extending π-

Downloaded from pubs.acs.org/acbcct/article-pdf/21/8/1891/6163245/acschembio.6c00300.pdf by UNIV OF CALIFORNIA IRVINE user on 06 November 2026

https://doi.org/10.1021/acschembio.6c00300
ACS Chem. Biol. 2026, 21, 1891−1896

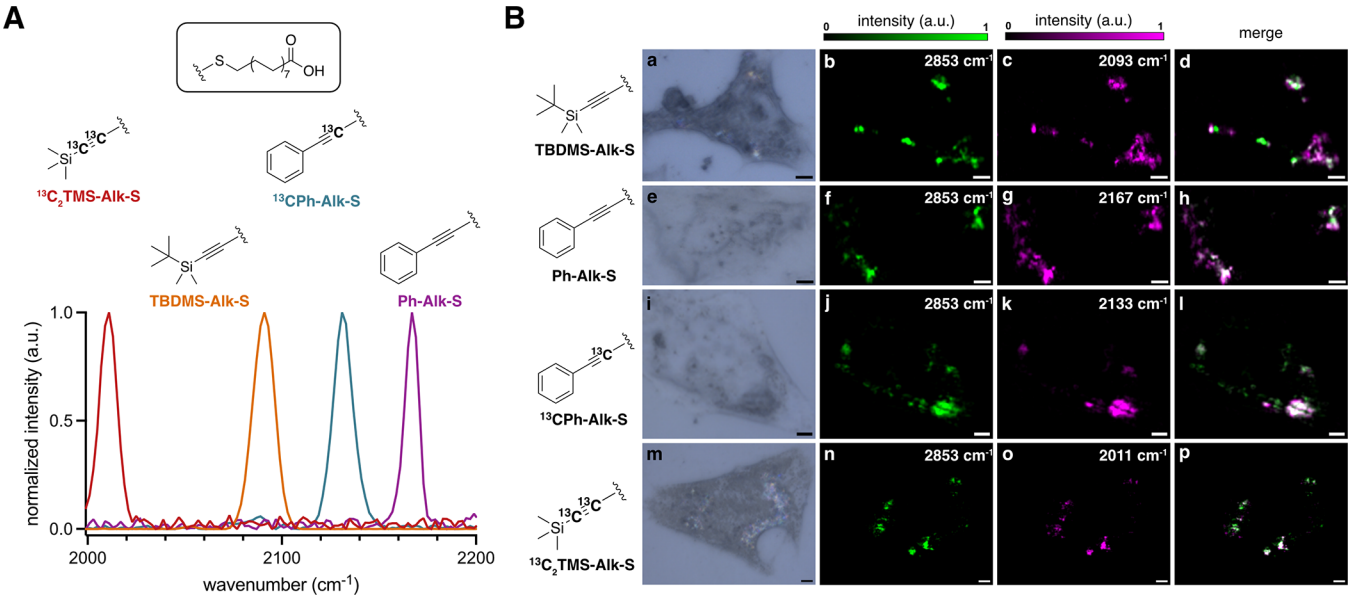


Figure 4. (A) IR measurements of optimized alkyne probes with four spectrally resolved signals: **$^{13}C_2$TMS-Alk-S**, **TBDMS-Alk-S**, **^{13}CPh-Alk-S**, **Ph-Alk-S**. (B) Brightfield images of labeled HeLa cells (a, e, i, m); OPTIR images acquired at the C(sp_3)-H stretching mode for lipid detection (b, f, j, n) and at the corresponding alkyne mode for individual tags (c, g, k, o); merged OPTIR images (d, h, l, p). Scale bars = 5 μm.

conjugation lowers electronic resonance, directly increasing Raman polarizability, yet it does not necessarily alter the IR transition dipole moment.

Second, n→π* bonding via a sulfur linker universally enhances both Raman and IR responses. The incorporation of a sulfur atom significantly improves IR activity across all examined motifs. By replacing the sulfur linker with a larger, more polarizable selenium atom, we observed a further ∼ 10 cm^{-1} red-shift, confirming that the linker atom can act as an additional "tuning knob" for the alkynyl vibrational frequency.

Third, we confirmed a substantial increase in the alkyne's IR response upon silyl termination. This activation is attributed to the donation of the alkyne's π-electron density into empty silicon d-orbitals. All silyl-terminated tags exhibited red-shifted resonances compared to terminal alkynes, indicating a weakened alkynyl bond consistent with this mechanism of IR activation.

Fourth, the mode frequency of aryl- and silyl-substituted alkynes remains remarkably robust against peripheral modifications. For example, introducing electron-withdrawing groups onto the phenyl ring failed to shift the alkyne frequency meaningfully. However, extending the conjugation, such as replacing phenyl with naphthalene, provided a significant spectral shift while maintaining narrow line widths. Similarly, while alkyl modifications to silyl groups had little effect, phenyl substitution on the silicon atom suggested that the silicon center effectively insulates the alkyne's electronic distribution from more distant substituents.

Fifth, isotopic labeling provided a proven orthogonal approach to frequency tuning. Substitution with ^{13}C atoms predictably red-shifted the alkyne stretch, enabling clear separation of otherwise overlapping peaks. Overall, by integrating conjugation extension, chalcogen substitution, and isotopic labeling, we established a palette of four distinct vibrational probes. The sharp, well-separated bands of these tags in the biologically silent window make them a helpful tool for IR-based imaging. Our OPTIR images demonstrate the utility of the tag palette, enabling the mapping of targeted biomolecules in cells with submicron resolution.

METHODS

General Synthetic Procedures

All reactions were run under an argon or nitrogen atmosphere at ambient temperature unless otherwise indicated. All reagents and solvents were used as received from the chemical suppliers, unless otherwise stated. Anhydrous organic solvents were prepared by degassing with argon and passing through two 4 in. x 36 in. columns of anhydrous neutral A-2 (LaRoche Chemicals, 8 × 14 mesh, activated at 350 °C for 12 h under a flow of argon). Organic solvents were removed under reduced pressure using a Büchi rotary evaporator. Column chromatography was performed using SiliaFlash F60 silica gel (SiliCycle, 60 Å pore size, 40−63 μm particle size). Thin-layer chromatography (TLC) was carried out with Silica Gel 60 F_{254}-coated glass plates (Merck Millipore, 60 Å pore size, 10−12 μm particle size, 250 μm thickness). TLC plates were visualized using UV light, $KMnO_4$ stain, or CAM stain.

^{1}H and ^{13}C NMR spectra were obtained using Bruker instruments: AVANCE NEO 400 and AVANCE NEO 500. ^{1}H spectra were acquired at 500 or 400 MHz, ^{19}F spectra were acquired at 470 or 376 MHz, and ^{13}C{^{1}H} spectra were acquired at 125 or 100 MHz. Spectra were internally referenced to residual solvent signals: 7.26 ppm for ^{1}H and 77.16 ppm for ^{13}C in $CDCl_3$. All spectra were acquired at 298 K. Chemical shifts are reported in ppm, and coupling constants (J) are reported in hertz (Hz). High-resolution mass spectrometry (HRMS) was performed at the University of California, Irvine Mass Spectrometry Facility using a Waters (Micromass) LCT Premier TOF LC/MS.

More detailed procedures and spectroscopic data for individual compounds are provided in the Supporting Information file.

Mammalian Cell Culture

HeLa cells were cultured in DMEM/high glucose media containing 10% fetal bovine serum (FBS), 1% penicillin/streptomycin, 4.5 g/L glucose, and 2 mM L-glutamine in 25 mL sterile vented cap tissue culture flasks.

Vibrational Probe Labeling

HeLa cells were incubated in DMEM/high glucose media (Corning) supplemented with 10% fetal bovine serum (FBS, Life Technologies)

https://doi.org/10.1021/acschembio.6c00300
ACS Chem. Biol. 2026, 21, 1891−1896

Downloaded from pubs.acs.org/acbcct/article-pdf/21/8/1891/6163245/acschembio.6c00300.pdf by UNIV OF CALIFORNIA IRVINE user on 06 November 2026

and 1% penicillin/streptomycin (Thermo-Fisher) in a 25 mL sterile vented cap culture flask. Synthesized vibrational probes were dissolved in 1 mL DMSO (Sigma-Aldrich), then further diluted using DMEM media to make a 200 μM solution. At 90% confluence, cells were trypsinized and replated on glass coverslips (18 mm diameter) in a 12-well plate. Cell suspension (100 μL) was added to each well, along with varying ratios of media and vibrational probe solutions (final concentration of probe ranged from 10−150 μM). For **TPS-Alk-S**, the compound solution was premixed with Lipofectamine 3000 (Thermo-Fisher) in a 10:1 ratio (Lipofectamine 3000:**TPS-Alk-S**) for 15 min prior to addition. Cells were incubated for 2−4 d on glass coverslips. Cells were then fixed with 4% paraformaldehyde (Thermo-Fisher) in PBS (15 min, RT), then washed twice with PBS. Cell samples were dried prior to imaging.

OPTIR Microscopy

IR-sensitive imaging was performed using a mIRage-LS infrared microscope (Photothermal Spectroscopy Corp.) equipped with a four-module pulse quantum cascade laser (QCL) system spanning the range from 932 cm^{-1} to 3205 cm^{-1}. Brightfield optical images were obtained using a 40x Cassegrain objective with a 0.78 numerical aperature. OPTIR images, IR, and Raman spectra of fixed cells were collected in copropagating mode using the same 40x Cassegrain in reflection mode. The MIR laser power was kept below 5 mW, and probe power was in the 10 mW range for all images collected. Acquisition time was 30−45 min per cell at 0.2 um per pixel, with a rate of 50−100 pixels per second. Images were taken at both resonant and off-resonant vibrational frequencies, with the latter serving as the background signal. To display the vibrationally resonant OPTIR images, the background was subtracted.

Stimulated Raman Scattering Imaging

The cell samples were covered with a coverslip and sealed with nail polish. The SRS imaging system consisted of an 80 MHz picosecond optical parametric oscillator (OPO, APE picoEmerald) synchronously pumped by the frequency-doubled output of a 4 ps, 1031 nm fiber laser (aeroPULSe, NKT Photonics). The residual 1031 nm beam was intensity modulated at 20 MHz and used as the Stokes beam. The OPO signal was tuned between 833−855 nm to provide the pump beam. Pump and Stokes pulses were temporally overlapped, collinearly combined on a dichroic mirror, and delivered into a laser-scanning microscope (Fluoview 300 coupled to IX71, Olympus). Excitation was focused on the sample using a 60×, 1.20 NA water-immersion objective (Olympus). The transmitted pump beam was collected in the forward direction with a 1.4 NA oil-immersion condenser (Olympus), filtered using a 960 nm short-pass filter, and detected with a wide-area photodiode. The resulting photocurrent was subsequently amplified and demodulated at 20 MHz with a lock-in amplifier (HF2LI, Zurich Instruments).

■ ASSOCIATED CONTENT

Supporting Information

The Supporting Information is available free of charge at https://pubs.acs.org/doi/10.1021/acschembio.6c00300.

Additional SRS images of cells, stability assays of probes, synthetic methods for alkynyl lipids, and NMR spectra (PDF)

■ AUTHOR INFORMATION

Corresponding Authors

Eric O. Potma − *Departments of Chemistry, University of California Irvine, Irvine 92697 California, United States;* orcid.org/0000-0003-3916-6131; Email: epotma@uci.edu

Jennifer A. Prescher − *Departments of Chemistry, Molecular Biology and Biochemistry, and Pharmaceutical Sciences, University of California Irvine, Irvine 92697 California, United States;* orcid.org/0000-0002-9250-4702; Email: jpresche@uci.edu

Authors

Halley M. Lin-Jones − *Departments of Chemistry, University of California Irvine, Irvine 92697 California, United States*

Tuyet Hoang − *Departments of Chemistry, University of California Irvine, Irvine 92697 California, United States*

Yong Li − *Departments of Chemistry, University of California Irvine, Irvine 92697 California, United States*

Katherine M. Townsend − *Departments of Chemistry, University of California Irvine, Irvine 92697 California, United States*

Shelbee K. Botello − *Departments of Chemistry, University of California Irvine, Irvine 92697 California, United States*

Complete contact information is available at: https://pubs.acs.org/10.1021/acschembio.6c00300

Author Contributions

H.M.L. and T.H. designed and conducted the experiments. S.K.B. contributed to compound synthesis. K.M.T. and Y.L. performed preliminary experiments and contributed to project design. J.A.P. and E.O.P. directed the research and writing. H.M.L. prepared the manuscript and figures, and all authors revised and approved the final version.

Notes

The authors declare the following competing financial interest(s): Prescher is an Associate Editor at ACS Chemical Biology.

■ ACKNOWLEDGMENTS

The authors acknowledge financial support from the National Science Foundation, Grant CBET-2013814 and CHE-2407328. Some of the experiments were performed with the help of the Laser Spectroscopy Laboratories, University of California, Irvine.

■ REFERENCES

(1) Sletten, E. M.; Bertozzi, C. R. Bioorthogonal Chemistry: Fishing for Selectivity in a Sea of Functionality. *Angew. Chem., Int. Ed.* **2009**, *48* (38), 6974−6998.

(2) Murrey, H. E.; Judkins, J. C.; Am Ende, C. W.; Ballard, T. E.; Fang, Y.; Riccardi, K.; Di, L.; Guilmette, E. R.; Schwartz, J. W.; Fox, J. M.; Johnson, D. S. Systematic Evaluation of Bioorthogonal Reactions in Live Cells with Clickable HaloTag Ligands: Implications for Intracellular Imaging. *J. Am. Chem. Soc.* **2015**, *137* (35), 11461−11475.

(3) Yamakoshi, H.; Dodo, K.; Okada, M.; Ando, J.; Palonpon, A.; Fujita, K.; Kawata, S.; Sodeoka, M. Imaging of EdU, an Alkyne-Tagged Cell Proliferation Probe, by Raman Microscopy. *J. Am. Chem. Soc.* **2011**, *133* (16), 6102−6105.

(4) Azemtsop Matanfack, G.; Rüger, J.; Stiebing, C.; Schmitt, M.; Popp, J. Imaging the Invisible—Bioorthogonal Raman Probes for Imaging of Cells and Tissues. *J. Biophotonics* **2020**, *13* (9), No. e202000129.

(5) Wei, L.; Hu, F.; Chen, Z.; Shen, Y.; Zhang, L.; Min, W. Live-Cell Bioorthogonal Chemical Imaging: Stimulated Raman Scattering Microscopy of Vibrational Probes. *Acc. Chem. Res.* **2016**, *49* (8), 1494−1502.

(6) Du, J.; Wang, H.; Wei, L. Bringing Vibrational Imaging to Chemical Biology with Molecular Probes. *ACS Chem. Biol.* **2022**, *17* (7), 1621−1637.

Downloaded from pubs.acs.org/acbcct/article-pdf/21/8/1891/6163245/acschembio.6c00300.pdf by UNIV OF CALIFORNIA IRVINE user on 06 November 2026

(7) Zhao, Z.; Chen, C.; Xiong, H.; Ji, J.; Min, W. Metabolic Activity Phenotyping of Single Cells with Multiplexed Vibrational Probes. *Anal. Chem.* **2020**, *92* (14), 9603−9612.
(8) Chen, C.; Zhao, Z.; Qian, N.; Wei, S.; Hu, F.; Min, W. Multiplexed Live-Cell Profiling with Raman Probes. *Nat. Commun.* **2021**, *12* (1), 3405.
(9) Law, S. S. Y.; Asanuma, M.; Shou, J.; Ozeki, Y.; Kodama, Y.; Numata, K. Deuterium- and Alkyne-Based Bioorthogonal Raman Probes for In Situ Quantitative Metabolic Imaging of Lipids within Plants. *JACS Au* **2023**, *3* (6), 1604−1614.
(10) Wei, L.; Chen, Z.; Shi, L.; Long, R.; Anzalone, A. V.; Zhang, L.; Hu, F.; Yuste, R.; Cornish, V. W.; Min, W. Super-Multiplex Vibrational Imaging. *Nature* **2017**, *544* (7651), 465−470.
(11) Hu, F.; Zeng, C.; Long, R.; Miao, Y.; Wei, L.; Xu, Q.; Min, W. Supermultiplexed Optical Imaging and Barcoding with Engineered Polyynes. *Nat. Methods* **2018**, *15* (3), 194−200.
(12) Nishiyama, R.; Hiramatsu, K.; Kawamura, S.; Dodo, K.; Furuya, K.; de Pablo, J. G.; Takizawa, S.; Min, W.; Sodeoka, M.; Goda, K. Color-Scalable Flow Cytometry with Raman Tags. *PNAS Nexus* **2023**, *2* (2), No. pgad001.
(13) Qian, N.; Zhao, Z.; El Khoury, E.; Gao, X.; Canela, C.; Shen, Y.; Shi, L.; Shi, L.; Hu, F.; Wei, L.; Min, W. Illuminating Life Processes by Vibrational Probes. *Nat. Methods* **2025**, *22* (5), 928−944.
(14) Lee, E. S.; Lee, J. Y. High Resolution Cellular Imaging with Nonlinear Optical Infrared Microscopy. *Opt. Express* **2011**, *19* (2), 1378.
(15) Zhang, D.; Li, C.; Zhang, C.; Slipchenko, M. N.; Eakins, G.; Cheng, J.-X. Depth-Resolved Mid-Infrared Photothermal Imaging of Living Cells and Organisms with Submicrometer Spatial Resolution. *Sci. Adv.* **2016**, *2* (9), No. e1600521.
(16) Teng, X.; Li, M.; He, H.; Jia, D.; Yin, J.; Bolarinho, R.; Cheng, J.-X. Mid-Infrared Photothermal Imaging: Instrument and Life Science Applications. *Anal. Chem.* **2024**, *96* (20), 7895−7906.
(17) Shi, L.; Liu, X.; Shi, L.; Stinson, H. T.; Rowlette, J.; Kahl, L. J.; Evans, C. R.; Zheng, C.; Dietrich, L. E. P.; Min, W. Mid-Infrared Metabolic Imaging with Vibrational Probes. *Nat. Methods* **2020**, *17* (8), 844−851.
(18) Bai, Y.; Camargo, C. M.; Glasauer, S. M. K.; Gifford, R.; Tian, X.; Longhini, A. P.; Kosik, K. S. Single-Cell Mapping of Lipid Metabolites Using an Infrared Probe in Human-Derived Model Systems. *Nat. Commun.* **2024**, *15* (1), 350.
(19) Liu, X.; Shi, L.; Zhao, Z.; Shu, J.; Min, W. VIBRANT: Spectral Profiling for Single-Cell Drug Responses. *Nat. Methods* **2024**, *21* (3), 501−511.
(20) Shuster, S. O.; Curtis, A. E.; Davis, C. M. Optical Photothermal Infrared Imaging Using Metabolic Probes in Biological Systems. *Anal. Chem.* **2025**, *97* (15), 8202−8212.
(21) He, H.; Yin, J.; Li, M.; Dessai, C. V. P.; Yi, M.; Teng, X.; Zhang, M.; Li, Y.; Du, Z.; Xu, B.; Cheng, J.-X. Mapping Enzyme Activity in Living Systems by Real-Time Mid-Infrared Photothermal Imaging of Nitrile Chameleons. *Nat. Methods* **2024**, *21* (2), 342−352.
(22) Li, Y.; Townsend, K. M.; Dorn, R. S.; Prescher, J. A.; Potma, E. O. Enhancing Alkyne-Based Raman Tags with a Sulfur Linker. *J. Phys. Chem. B* **2023**, *127* (9), 1976−1982.
(23) Kossowska, D.; Park, K.; Park, J. Y.; Lim, C.; Kwak, K.; Cho, M. Rational Design of an Acetylenic Infrared Probe with Enhanced Dipole Strength and Increased Vibrational Lifetime. *J. Phys. Chem. B* **2019**, *123* (29), 6274−6281.
(24) Stiebing, C.; Meyer, T.; Rimke, I.; Matthäus, C.; Schmitt, M.; Lorkowski, S.; Popp, J. Real-time Raman and SRS Imaging of Living Human Macrophages Reveals Cell-to-cell Heterogeneity and Dynamics of Lipid Uptake. *J. Biophotonics* **2017**, *10* (9), 1217−1226.

Downloaded from pubs.acs.org/acbcct/article-pdf/21/8/1891/6163245/acschembio.6c00300.pdf by UNIV OF CALIFORNIA IRVINE user on 06 November 2026

https://doi.org/10.1021/acschembio.6c00300
ACS Chem. Biol. 2026, 21, 1891−1896